Simulation of Ca^{2+} persistent inward currents in spinal motoneurones: mode of activation and integration of synaptic inputs

Sherif M. ElBasiouny[1,2], David J. Bennett[1,2,3] and Vivian K. Mushahwar[1,2]

[1]*Department of Biomedical Engineering and* [2]*Centre for Neuroscience, Faculty of Medicine and Dentistry, and* [3]*Faculty of Rehabilitation Medicine, University of Alberta, Edmonton, Alberta, Canada*

The goal of this study was to investigate the nature of activation of the dendritic calcium persistent inward current (Ca^{2+} PIC) and its contribution to the enhancement and summation of synaptic inputs in spinal motoneurones. A compartmental cable model of a cat α-motoneurone was developed comprising the realistic dendritic distribution of Ia-afferent synapses and low-voltage-activated L-type calcium ($Ca_v1.3$) channels distributed over the dendrites in a manner that was previously shown to match a wide set of experimental measurements. The level of synaptic activation was systematically increased and the resulting firing rate, somatic and dendritic membrane potentials, dendritic $Ca_v1.3$ channel conductance, and dendritic Ca^{2+} PIC were measured. Our simulation results suggest that during cell firing the dendritic Ca^{2+} PIC is not activated in an all-or-none manner. Instead, it is initially activated in a graded manner with increasing synaptic input until it reaches its full activation level, after which additional increases in synaptic input result in minimal changes in the Ca^{2+} PIC (PIC saturated). The range of graded activation of Ca^{2+} PIC occurs when the cell is recruited and causes a steep increase in the firing frequency as the synaptic current is increased, coinciding with the secondary range of the synaptic frequency–current (*F–I*) relationship. Once the Ca^{2+} PIC is saturated the slope of the *F–I* relationship is reduced, corresponding to the tertiary range of firing. When the post-spike after-hyperpolarization (AHP) is blocked, either directly by blocking the calcium-activated potassium channels, or indirectly by blocking the sodium spikes, the PIC is activated in an all-or-none manner with increasing synaptic input. Thus, the AHP serves to limit the depolarization of the cell during firing and enables graded, rather than all-or-none, activation of the Ca^{2+} PIC. The graded activation of the Ca^{2+} PIC with increasing synaptic input results in a graded (linear) enhancement and linear summation of synaptic inputs. In contrast, the saturated Ca^{2+} PIC enhances synaptic inputs by a constant amount (constant current), and leads to less-than linear summation of multiple synaptic inputs. These model predictions improve our understanding of the mode of activation of the dendritic Ca^{2+} PIC and its role in the enhancement and integration of synaptic inputs.

(Received 21 September 2005; accepted after revision 15 November 2005; first published online 24 November 2005)
Corresponding author V. K. Mushahwar: 513 Heritage Medical Research Center, Department of Biomedical Engineering, Centre for Neuroscience, University of Alberta, Edmonton, Alberta, Canada T6G 2S2.
Email: vivian.mushahwar@ualberta.ca

The finding of voltage-gated ion channels on the dendritic tree of spinal motoneurones has changed the classical view of dendrites as being passive structures. This classical view was supported by the linear summation of synaptic inputs reported from early motoneurone experimental recordings obtained from anaesthetized animal preparations (Granit *et al.* 1966*a*). It is now believed that dendrites of motoneurones are active structures that have ionic conductances which play a fundamental role in shaping the motor output. The ionic conductances, especially those mediating persistent inward currents (PICs), when activated generate sustained depolarization of the membrane causing plateau potentials (Hounsgaard *et al.* 1988). They also amplify synaptic currents three to six times at potentials close to the voltage threshold for firing (Lee *et al.* 2003). The enhancement of synaptic currents by these PIC-mediating channels explains the inconsistency between the strength of synaptic current

© 2006 The Authors. Journal compilation © 2006 The Physiological Society DOI: 10.1113/jphysiol.2005.099119

reaching the soma and the resulting motoneurone firing rates (Rose & Cushing, 1999; Powers & Binder, 2001).

The question of whether PICs and plateau potentials are activated in a graded or all-or-none manner has recently received much attention (for example: Hultborn *et al.* 2003; Lee *et al.* 2003); however, the answer to this question remains unclear. The difficulty in inferring the mode of activation of the dendritic PIC comes from the discrepancies in experimental results leading to inconsistent explanations of the behaviour of the PIC. For example, synaptic input provided by smooth muscle stretch caused a graded increase in motoneurone firing rate before saturation (Lee *et al.* 2003) suggesting graded activation of the PIC. However, in the same study, a step increase in firing rate was also seen in some motoneurones suggesting all-or-none activation of the PIC (Lee *et al.* 2003). In current-clamp experiments where the spikes were blocked, the membrane potential was found to jump abruptly into a state of sustained depolarization (plateau potentials) when the PIC was activated, suggesting an all-or-none activation of the PIC as well (Hounsgaard *et al.* 1988; Bennett *et al.* 1998; Lee & Heckman, 1999).

Discrepancies have also been reported regarding the role of the PIC in enhancing and integrating synaptic inputs. In examining the enhancement of synaptic currents by the effect of PIC, Hultborn *et al.* (2003) reported graded (variable) enhancement of synaptic inputs as the PIC is activated in experimental recordings obtained from decerebrate cat motoneurones. Prather *et al.* (2001), on the other hand, reported constant enhancement of synaptic inputs by the PIC (indicated by a vertical shift in the frequency–current (*F–I*) relationship relative to that predicted when the synaptic input was applied) in decerebrate cat motoneurones as well. Because of the effect of the dendritic PIC on the enhancement of synaptic inputs, non-linear summation of multiple synaptic inputs was expected (Powers & Binder, 2001). However, linear summation (Burke, 1967; Prather *et al.* 2001), less-than linear summation (Kuno & Miyahara, 1969), and even occasionally greater-than linear summation (Powers & Binder, 2000) of synaptic inputs have been reported.

The primary reason for the existence of these unresolved discrepancies in experimental reports is the inability to record directly the dendritic currents in experimental setups. Thus, the goal of the present study is to examine the mode of activation of the Ca^{2+} PIC in spinal motoneurones using computer simulations, and examine its role in the production of cell firing, and in the enhancement and summation of synaptic inputs. For the purposes of this paper, we define all-or-none activation as an abrupt transition from a state of no PIC activation to a state of full PIC activation in response to a small increase in synaptic current (in steady state). In other words, a discontinuity in the activation profile of the PIC will be seen with respect to the change in synaptic current. In contrast, graded activation is defined as small increases in PIC activation in response to successive small increases in synaptic current. To quantify the *F–I* relationship, we use the classical nomenclature for describing the different piece-wise linear ranges of cell firing in response to current injection at the soma (primary, secondary and tertiary ranges), as originally defined by Kernell (1965*a*,*b*). We also extend the use of this nomenclature to describe the piece-wise linear firing ranges in response to *synaptic* activation (Granit *et al.* 1966*a*,*b*; Heckman & Binder, 1988).

A compartmental cable model of a cat α-motoneurone comprising the dendritic low-voltage-activated (LVA) L-type calcium ($Ca_v1.3$) channels and the realistic dendritic distribution of Ia-afferent synapses, which was previously developed and verified (ElBasiouny *et al.* 2005*b*), was used to examine these behaviours. This made the evaluation of the dendritic Ca^{2+} PIC possible since dendritic recordings are generally difficult in real motoneurones. The synaptic input to the motoneurone was linearly increased while cell firing, somatic and dendritic membrane potentials, dendritic $Ca_v1.3$ channel conductance, and dendritic Ca^{2+} PIC were simultaneously measured. The modes of activation of the Ca^{2+} PIC were investigated under three conditions: (1) during spike blockage; (2) under voltage-clamp conditions; and (3) during normal cell firing. The role of the Ca^{2+} PIC in the enhancement and summation of synaptic inputs was then assessed and explained in light of its distinct modes of activation. Our simulations suggest that during normal firing Ca^{2+} PIC is not activated in an all-or-none manner; rather, it is activated in two stages. The Ca^{2+} PIC is first activated in a graded fashion in response to increasing synaptic input causing the cell to fire in its secondary range. The Ca^{2+} PIC then becomes fully activated (saturated) and no additional increase in its amplitude is achieved in response to more synaptic input. This saturated stage corresponds to the tertiary range of cell firing (Li *et al.* 2004). No all-or-none activation of the Ca^{2+} PIC occurs during cell firing due to the subthreshold clamping effect of the post-spike afterhyperpolarization (AHP) on the membrane potential, which limits the extent of Ca^{2+} PIC activation. During the graded phase of Ca^{2+} PIC activation, the PIC causes a graded (linear) enhancement of the synaptic inputs in proportion to the level of synaptic excitation, whereas when the Ca^{2+} PIC is saturated it enhances synaptic inputs by a constant amount (i.e. constant current) in proportion to the level of synaptic excitation. During the secondary range of firing where the Ca^{2+} PIC is graded, synaptic inputs sum linearly. Conversely, during the tertiary range of firing where the Ca^{2+} PIC is saturated, synaptic inputs sum less-than linearly. Part of this work has been previously

© 2006 The Authors. Journal compilation © 2006 The Physiological Society

presented in abstract form (ElBasiouny & Mushahwar, 2004; ElBasiouny *et al.* 2005*a*).

Methods

Model description

A full description of the model morphology, biophysical properties, and its verification is provided in ElBasiouny *et al.* (2005*b*). Briefly, a computer-based cable model of an adult cat α-motoneurone was developed using the NEURON simulation environment (Hines & Carnevale, 1997). The model had full representation of the α-motoneurone structure, and consisted of soma, axon hillock, initial segment and dendritic tree. The model dendritic tree was based on the three-dimensional detailed morphology for type-identified triceps surae α-motoneurone (fatigue-resistant (FR) type, medial gastrocnemius (MG) motoneurone, identified as cell 43/5), labelled intracellularly with horseradish peroxidase (Cullheim *et al.* 1987). The model *passive* properties were set based on previous studies for the same 43/5 FR motoneurone (Cullheim *et al.* 1987; Fleshman *et al.* 1988). Voltage-gated ion channels (fast Na^+, persistent Na^+, delayed rectifier K^+, Ca^{2+}-activated K^+ and N-type Ca^{2+}) were then set such that the model properties were within the 95% confidence range of experimental data, and the model generated action potentials and afterhyperpolarizations (AHPs) with properties similar to experimental recordings (Table 2 in ElBasiouny *et al.* 2005*b*). Furthermore, the model exhibited adaptation of firing rate that was similar to experimental data when long current pulses were injected into the soma (Sawczuk *et al.* 1995; not illustrated).

$Ca_v1.3$ channels

Low-voltage-activated (LVA) L-type calcium ($Ca_v1.3$-type) channels were then distributed on the dendritic tree based on the *wide band distribution* previously described in ElBasiouny *et al.* (2005*b*). In this distribution, the $Ca_v1.3$ channels were localized on dendritic segments with dendritic path distance between 300 μm and 850 μm from the soma, which is the dendritic region mostly covered by the Ia-afferent synapses. With this distribution, the model matched different and independent sets of experimental measurements from cat motoneurones innervating the MG muscle. These measurements were: (a) properties of Ca^{2+} PIC and *F–I* relationship; (b) changes in the somatic plateau threshold and *F–I* relationship due to background synaptic activity; (c) enhancement of Ia-synaptic current; (d) shape and timing of tail currents seen experimentally at the termination of long voltage pulses; and (e) changes in the shape of AHP after the activation of the Ca^{2+} PIC (ElBasiouny *et al.* 2005*b*).

Dendritic synaptic inputs and their graded activation

The monosynaptic Ia-afferent system was represented in the model. The dendritic spatial distribution of Ia-afferent synapses was based on the realistic distribution of group Ia afferent-to-motoneurone contacts from cat FR motoneurones (Burke *et al.* 1979; Glenn *et al.* 1982; Burke & Glenn, 1996). It is noteworthy that synaptic inputs from other systems appear to have a similar distribution to that of Ia-afferents (Segev *et al.* 1990; Fyffe, 1991; Brannstrom, 1993; Burke & Glenn, 1996). Tendon vibration was simulated by activating the Ia-afferent synapses at 180 Hz while adjusting the synapse conductances to give a Ia effective synaptic current (Ia I_N) of 4.8 nA at resting potential, which is the experimental value reported by Lee & Heckman (2000). This provided the effective synaptic conductance associated with the Ia I_N. The synapses were activated asynchronously as described by ElBasiouny *et al.* (2005*b*).

To allow for systematic gradation of the synaptic input, the total number of Ia-synapses was divided into eight nearly equal groups, randomly distributed on the dendrites (ElBasiouny *et al.* 2005*b*). The Ia-synaptic groups were sequentially activated (from 14 to 100%) such that the maximum magnitude of Ia I_N was equal to that obtained experimentally when all Ia-synapses were activated (Ia $I_N = 4.8$ nA at 100% of synaptic excitation). This synaptic input resulted in a linear increase in the Ia I_N (measured at resting potential, –70 mV; Heckman & Binder, 1988) reaching the soma as more synapses were activated (Fig. 1). Given that the distribution of all synaptic inputs appears to be effectively similar (for discussion see ElBasiouny *et al.* 2005*b*), synaptic input from systems other than the Ia-afferents was simulated by increasing the synapse conductances to generate higher synaptic currents (over 100% of synaptic excitation), and this again resulted in a linear increase in the Ia I_N reaching the soma (Fig. 1).

Measurement of dendritic Ca^{2+} PIC and its conductance

While plateau potentials are commonly seen experimentally in a variety of motoneurones, their mode of activation and level of gradability have been difficult to assess. To address this question, simulations were run under three conditions: (1) during spike blockage; (2) under voltage-clamp conditions; and (3) during normal cell firing. For each condition, we systematically increased the level of synaptic activation (as described above) and then measured, from the soma, the somatic membrane potential, firing rate,

© 2006 The Authors. Journal compilation © 2006 The Physiological Society

and the leak-subtracted Ca^{2+} PIC as seen from the soma under voltage-clamp conditions (e.g. Fig. 3). We also calculated the average/filtered somatic membrane potential during firing by applying a low pass filter (corner frequency = 1 Hz) which effectively provides the level of somatic membrane potential without spikes, i.e. potential seen by the slow Ca^{2+} PIC (e.g. Fig. 4*B*). The dendritic Ca^{2+} PIC flowing in the $Ca_v1.3$ channels of a dendritic compartment located 695.9 μm from the soma (e.g. Figs 2*A* and 4*D*) and the dendritic membrane potential of the same compartment (e.g. Figs 2*A* and 4*C*) were directly measured in the model. We also assessed the level of activation of the $Ca_v1.3$ channels by measuring the overall conductance of the $Ca_v1.3$ channels on the dendritic tree (G_{Ca}, e.g. Fig. 4*E*). This overall conductance was computed as follows:

$$G_{Ca} = 1/n \times \sum_{i=1}^{n} g_{Ca_i}$$

where n is the number of compartments that have the $Ca_v1.3$ channels, and g_{Ca_i} is the conductance of the $Ca_v1.3$ channels in compartment number i.

Enhancement of synaptic inputs

The enhancement of synaptic current by the Ca^{2+} PIC was examined under voltage-clamp conditions. The synaptic current was computed as the difference between the current–voltage (I–V) relationships during no synaptic activity and during synaptic excitation. At the resting membrane potential (−70 mV), the difference between the I–V relationships was called the 'hyperpolarized Ia I_N', and represented the raw synaptic current with no Ca^{2+} PIC activation. The difference between the I–V relationships was maximum near threshold (−55 mV). This was called the 'peak Ia I_N', and represented the synaptic current enhanced by the Ca^{2+} PIC (Lee & Heckman, 2000). The difference between the peak Ia I_N and hyperpolarized Ia I_N provided the amount of augmentation in synaptic current caused by the activation of Ca^{2+} PIC at different levels of synaptic excitation (e.g. Fig. 6*D*).

Summation of synaptic inputs

We investigated the influence of activating multiple synaptic inputs on the activation level of the Ca^{2+} PIC, and how these inputs summed. The cell was initially induced to fire with a bias current to produce a steady low background firing level. Two different approaches were used to activate the cell to obtain background firing: synaptic activation (Fig. 8*A*), and intracellular current injection at the soma as in Prather *et al.* (2001; Fig. 8*D*). Two additional synaptic inputs (test synaptic inputs, termed A and B) were then applied. The magnitude of the two test synaptic inputs A and B was increased incrementally. Summation was then investigated by comparing the change in firing rate (relative to background) evoked by the concurrent activation of the two test synaptic inputs to the linear sum of changes in firing rates evoked by the individual activation of each test synaptic input (following the methods of Prather *et al.* 2001). The change in firing rate was computed as the difference between the background firing rate and the *steady-state* firing rate during activation of the test synaptic inputs.

Synapses on the dendritic tree were divided into three groups to provide the small synaptic bias current and the two test synaptic inputs (A and B). Each group had a dendritic distribution similar to that of the Ia-afferent system. Synapses of each group were activated at 180 Hz in order to provide synaptic excitation as described earlier, and their conductance was sequentially increased to provide an increasing effective synaptic current at the soma.

Results

The primary goal of this study was to investigate the nature of activation of the Ca^{2+} PIC, and assess its role in the generation of cell firing, and the enhancement and summation of synaptic inputs. Our previous simulation studies (ElBasiouny *et al.* 2005*b*) suggested that the $Ca_v1.3$ channels are primarily localized within the region of synaptic territory. This raised questions about the degree of dependence of Ca^{2+} PIC on the level of synaptic excitation, and whether Ca^{2+} PIC is activated in a graded or all-or-none manner. Furthermore, the resultant effect of PIC activation on synaptic current enhancement was in question.

Effective synaptic current

To address these questions, we systematically increased the level of synaptic excitation through Ia-afferent terminals by sequential activation of the Ia-synapses, as described in Methods. This synaptic input resulted in a linear increase in the Ia I_N reaching the soma as more synapses were activated (Fig. 1). The Ia I_N was measured with the somatic membrane potential clamped at −70 mV under voltage-clamp conditions, so that the PIC could not be activated, thus this current represents the raw synaptic current without activation of the Ca^{2+} PIC. Given that synaptic inputs from other systems appear to have a similar distribution to that of Ia-afferents (for discussion see ElBasiouny *et al.* 2005*b*), synaptic input up to 100% in Fig. 1 represented the input from the Ia-afferent system, whereas synaptic input over 100% represented the input from the many other presynaptic systems converging on motoneurones (Powers & Binder, 2000).

© 2006 The Authors. Journal compilation © 2006 The Physiological Society

Activation of the Ca^{2+} PIC during spike blockage

We first examined the activation of the Ca^{2+} PIC in the model with the sodium spikes blocked since real motoneurones have been extensively studied in the presence of sodium channel blockers, such as tetrodotoxin (TTX) (e.g. Hounsgaard & Kiehn, 1989; Li & Bennett, 2003), and the lidocaine (lignocaine) derivative QX-314 (e.g. Lee & Heckman, 1999). In current-clamp mode, we simultaneously measured the dendritic Ca^{2+} PIC, the somatic and dendritic membrane potential, and the overall conductance of the $Ca_v1.3$ channels (G_{Ca}) at different levels of synaptic excitation (Fig. 2). $Ca_v1.3$ channels were found to be activated in two stages during increasing synaptic input. In the first stage, the channels were gradually activated in response to the level of synaptic excitation resulting in a gradual change in G_{Ca}, Ca^{2+} PIC and membrane potential (traces a to b in Fig. 2*A* and *B*). The range of voltage over which the grading occurred corresponded to the range of voltage in the *I–V* relationship that was subthreshold to when a negative slope region (NSR) occurred (i.e. membrane potentials $<$ the onset potential, V_{on}, of the Ca^{+2} PIC). Once an adequate amount of synaptic excitation was reached, an all-or-none activation of the $Ca_v1.3$ channels took place, and resulted in a step increase in G_{Ca} (jump) and the generation of plateau potentials (see the jump from b to c in Fig. 2*A* and *B*). After that jump, G_{Ca} was saturated at its maximum value causing sustained depolarization in the membrane potential (plateau potentials; traces c to d in Fig. 2*A* and *B*). A minimum effective synaptic current of 5.4 nA was needed to trigger plateau potentials (vertical dashed line in Fig. 2*B*). Higher levels of synaptic excitation resulted in a faster activation of plateau potentials (Fig. 2*A*). The change in magnitude of G_{Ca} with respect to the increase in synaptic current showed an abrupt transition indicating an all-or-none activation of the Ca^{2+} PIC (Fig. 2*B*, lower graph). At the soma, this all-or-none activation corresponded to the jump in membrane potential from the 1st zero-slope point (V_{on}) on the *I–V* relationship to point c (in Fig. 2*C*) which allowed it to cross the unstable NSR created by the Ca^{2+} PIC (Schwindt & Crill, 1977). In summary, without spiking an increasing synaptic input initially activates the Ca^{2+} PIC in a graded manner, followed by an all-or-none increase to a level at which the Ca^{2+} PIC becomes saturated. This results in all-or-none generation of plateau potentials.

Activation of the Ca^{2+} PIC under voltage-clamp conditions

We next investigated the mode of activation of the Ca^{2+} PIC under conditions where the spiking mechanism was unblocked, but the somatic membrane potential was controlled with a voltage clamp at the soma. Such voltage clamp has been extensively used to measure the PICs directly (e.g. Lee & Heckman, 1998*b*), but is not equivalent to the physiological situation where the cell is free to fire. Two voltage-clamp commands are usually used for experimental measurement of PICs: (1) long voltage pulses (1 s or more); and (2) a slow ramp voltage command. Long voltage pulses provide steady-state current responses, but require a relatively long time to obtain the recordings, whereas with a slow voltage ramp command (of slope around 4 mV s^{-1}) current measurements are relatively close to steady-state values and are obtained in a much shorter period. Figure 3*A* (upper graph) illustrates the difference between the *I–V* relationships obtained by using these two voltage commands in our model. With long voltage pulses, the activation threshold of the Ca^{2+} PIC was hyperpolarized by 2 mV, on average, from that measured during a ramp voltage command. Under these voltage-clamp conditions, $Ca_v1.3$ channels were found to be activated in a graded manner. In other words, with long voltage pulses of increasing amplitude steady-state current responses were obtained in the NSR of the *I–V* relationship (Fig. 3*A*, filled circles), and no abrupt activation of $Ca_v1.3$ channels occurred within that range. G_{Ca} and leak-subtracted Ca^{2+} PIC measurements from the model also showed incremental increases in magnitude within the NSR, and saturated afterwards (Fig. 3*A*, middle and lower graphs).

The graded activation of the Ca^{2+} PIC with increasing somatic voltage was maintained when a steady synaptic input was provided during the voltage-clamp simulations (a–d in Fig. 3*B*). When the steady synaptic input was gradually increased, the voltage threshold for activating the Ca^{2+} PIC from the soma gradually decreased (horizontal line in Fig. 3*B*), and the Ca^{2+} PIC amplitude at a given holding potential gradually increased (vertical line in Fig. 3*B*). The graded activation of Ca^{2+} PIC at a fixed

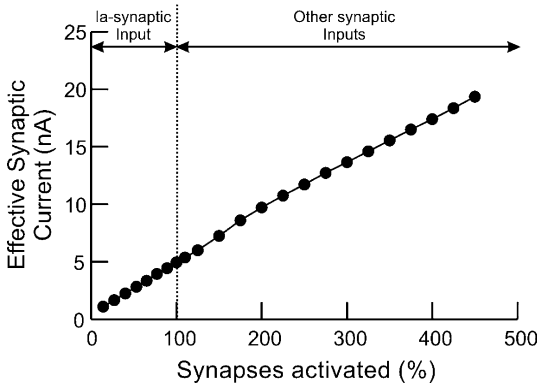

Figure 1. Effective synaptic current, measured at resting potential (–70 mV), reaching the soma at different levels of synaptic excitation (14–450%)
Sequential activation of a larger number of Ia-synaptic groups resulted in a linear increase in the effective synaptic current reaching the soma. Synapses activated above 100% represent inputs from systems other than the Ia-afferent system.

© 2006 The Authors. Journal compilation © 2006 The Physiological Society

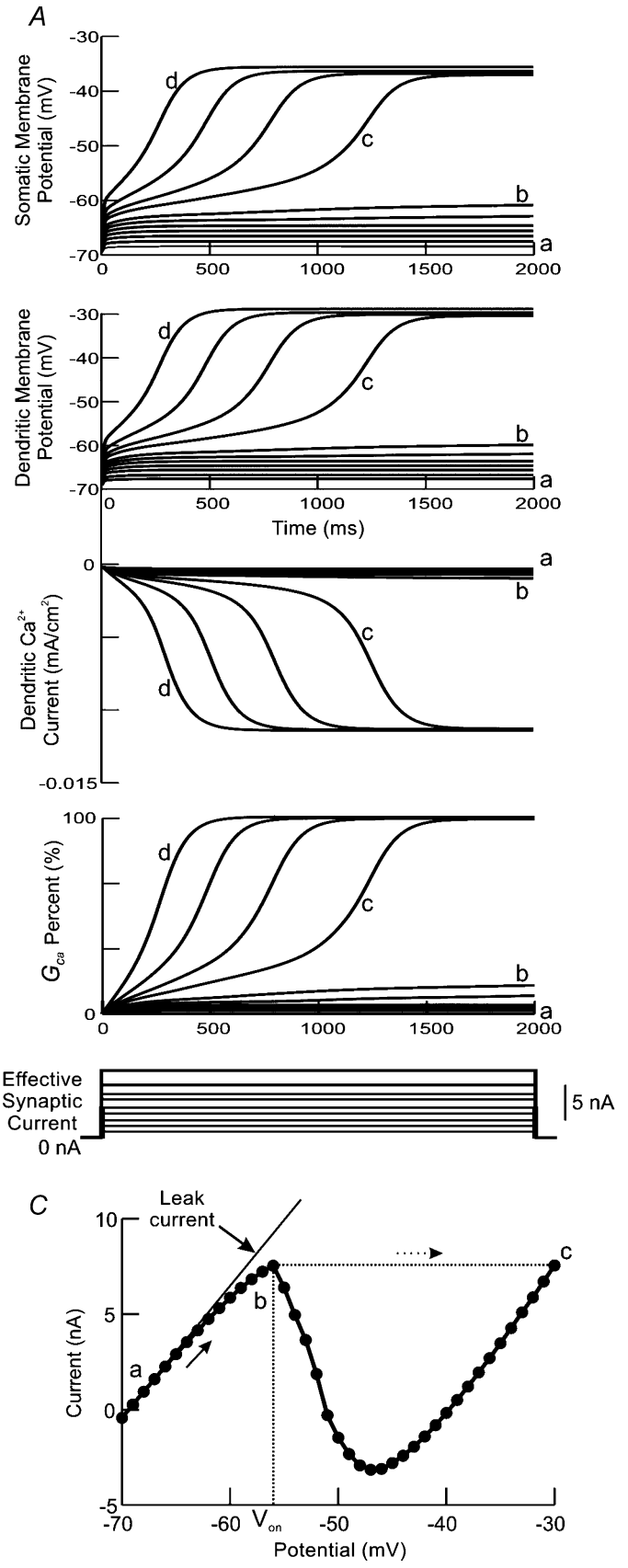

© 2006 The Authors. Journal compilation © 2006 The Physiological Society

potential occurred even when the membrane was in the unstable NSR of the steady-state *I–V* relationship. Correspondingly, the change in magnitude of G_{Ca} at different membrane potentials was always graded and no abrupt change in G_{Ca} occurred, further (Fig. 3*C*) suggesting that under voltage-clamp conditions, the Ca^{2+} PIC could remain partially activated by synaptic inputs, despite the presence of a NSR. In summary, when the somatic membrane is voltage-clamped at a given potential and the synaptic input is increased, the Ca^{2+} PIC is always activated in a graded manner even when the potential is in the NSR of the *I–V* relationship.

Activation of the Ca^{2+} PIC during normal cell firing

Activation of the Ca^{2+} PIC was then investigated under physiological conditions where the spike was not blocked and the cell was free to fire (with no current injected into the soma) in response to increasing synaptic input. We measured the magnitude of the dendritic Ca^{2+} PIC, dendritic G_{Ca}, cell firing rate, and membrane potential from the soma and a dendritic compartment at different levels of synaptic excitation applied for 2 s during normal firing (Fig. 4). The cell firing behaviour was found to be greatly affected by the activation of the $Ca_v1.3$ channels. For a given level of synaptic excitation, the dendritic $Ca_v1.3$ channels were gradually activated (Fig. 4*E*) causing a gradual increase in the magnitude of the Ca^{2+} PIC (Fig. 4*D*) that resulted in subthreshold depolarization (Fig. 4*B* and *C*) and early acceleration of cell firing rate just after recruitment (Fig. 4*A*). Note that adaptation in firing rate is not seen at relatively high synaptic inputs due to the activation of the Ca^{2+} PIC which tends to increase the firing rate. Given that the Ia I_N for the Ia-afferent system is 4.8 nA and cell firing starts at 4.9 nA (100% in Fig. 4*B*), the Ia-afferent system on its own is barely able to recruit FR motoneurones, as expected (Bennett *et al.* 1998; Lee & Heckman, 1998*a*; Powers & Binder, 2000). Firing rates at synaptic excitation levels larger than 100% represent the effect of synaptic input from systems other than the Ia-afferents. Note that the relatively high firing rates seen in Fig. 4*A* are attributable to the fact that the modelled cell is an FR motoneurone.

The acceleration in cell firing rate (Fig. 4*A*) had a time course very similar to that of the increase in dendritic G_{Ca} (Fig. 4*E*) and experienced a slow increase over the initial 800 ms. Just prior to recruitment, the G_{Ca} began to increase sharply, but upon the onset of cell firing the rate of increase of G_{Ca} was abruptly decreased (indicated by the notches in Fig. 4*E*) due to the hyperpolarization of the membrane potential during the post-spike AHPs. These AHPs effectively clamped the soma membrane potential below the firing threshold (similar to the effect of voltage clamp described above). The clamping effect of the AHP on the somatic membrane potential was also evident in Fig. 4*B* as the filtered membrane potential was reduced upon the initiation of cell firing. The filtered potential was obtained by low pass filtering the membrane potential at 1 Hz to remove the spikes that do not affect the slow Ca^{2+} PIC.

To demonstrate that the AHP plays a critical role in clamping the potential below the firing level, hence limiting G_{Ca}, the effect of the AHP on cell firing was further examined by blocking the calcium-activated potassium channels (K(Ca)), which are responsible for the AHP, during simulations of synaptic activation (Fig. 5). In response to the same level of synaptic excitation (150%), steady-state firing rate was increased from 26.4 to 197 impulses s^{-1} after blocking the K(Ca) channels (Fig. 5*C*). The acceleration in firing rate was also much faster after blocking the K(Ca) channels indicating that Ca^{2+} PIC was activated more rapidly than in the presence of the K(Ca) channels. This rapid and high activation of the Ca^{2+} PIC is also evident from the profile of G_{Ca} (Fig. 5*D*). After blocking the K(Ca) channels, G_{Ca} increased steeply upon recruitment and saturated at nearly 93% of its magnitude indicating full activation of the Ca^{2+} PIC, whereas before blocking the K(Ca) channels, G_{Ca} increased

Figure 2. Direct measurements from the soma and a dendritic compartment during spike blockage at different levels of synaptic excitation
A, simultaneous measurements from the model of the somatic (upper graph) and dendritic (2nd graph) membrane potentials, dendritic Ca^{2+} persistent inward current (PIC) (3rd graph), and overall $Ca_v1.3$ channel conductance (G_{Ca}) (lower graph) at different levels of synaptic excitation. Traces show the responses for 14–200% in an ascending order of level of synaptic excitation (14%, 27%, 40%, 53%, 65%, 77%, 89%, 110%, 125%, 150% and 200%). The letters a, b, c and d show the responses at 14%, 89%, 110% and 200% of synaptic excitation, respectively. *B*, steady-state responses, measured at the end of a 2 s period of synaptic excitation in the traces shown in *A*, are plotted as a function of synaptic excitation level. The top axis shows the percentage of activated synapses at each level. Vertical dashed line shows the current level at which plateau potentials were triggered by synaptic excitation, which is equal to 5.4 nA. Horizontal dashed line shows the voltage threshold at which plateau potentials were triggered by graded synaptic excitation alone, which is equal to –60 mV. *C*, steady-state *I–V* relationship at the soma with a NSR created by the Ca^{2+} PIC. Thin continuous line shows the leak current. Vertical dashed line shows the 1st zero-slope point, or the onset potential (V_{on}) of the Ca^{2+} PIC. Solid arrow shows the direction of change in somatic current for an increasing level of membrane potential. Dashed arrow shows the jump in membrane potential to cross the NSR.

© 2006 The Authors. Journal compilation © 2006 The Physiological Society

more gradually upon recruitment and saturated at only 40% of its magnitude indicating partial activation of the Ca^{2+} PIC. Thus, no graded activation of the Ca^{2+} PIC occurred when the K(Ca) channels were blocked. Furthermore, the filtered somatic membrane potential was −57.5 mV before blocking the K(Ca) channels and −44.5 mV after their blockage (Fig. 5*E*). The change in magnitude of G_{Ca} with respect to synaptic current before and after blocking the K(Ca) channels at different levels of synaptic excitation (from 14% to 400%) is shown in Fig. 5*F*. Before blocking the K(Ca) channels, gradual increase in G_{Ca} was obtained in response to increasing synaptic inputs indicating a graded activation of the Ca^{2+} PIC (Fig. 5*F*, triangles), whereas an abrupt transition in G_{Ca} was obtained after blocking the K(Ca) channels indicating an all-or-none activation of the Ca^{2+} PIC

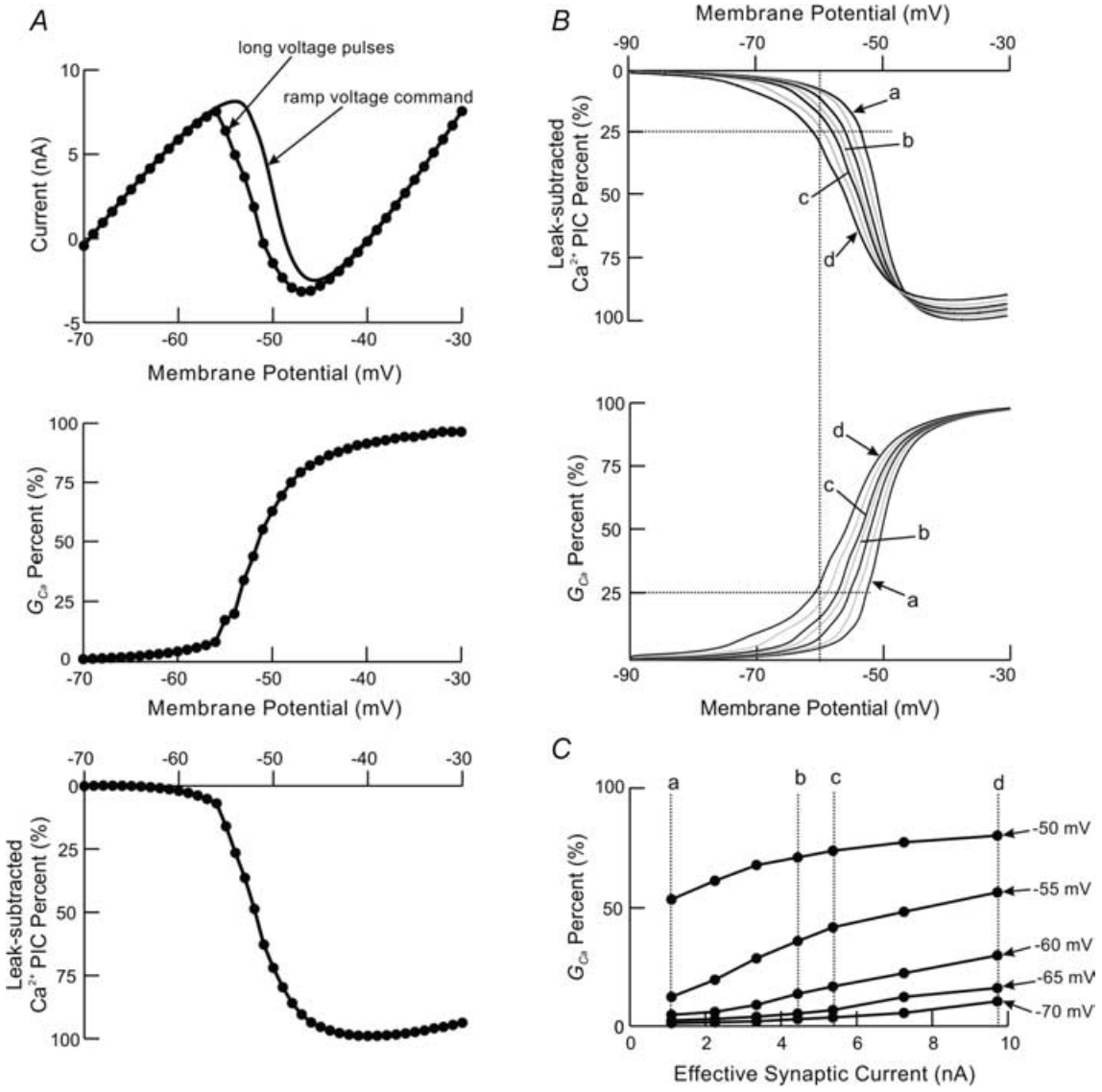

Figure 3. Measurements from the soma under voltage-clamp conditions for different levels of synaptic excitation

A, comparison of *I–V* relationships (upper graph) obtained by using a ramp voltage command (continuous line) and long voltage pulses (filled circles) with no synaptic activation. G_{Ca} (middle graph) and leak-subtracted Ca^{2+} PIC (lower graph) normalized to their peak values measured during long voltage pulses. *B*, leak-subtracted Ca^{2+} PIC (upper graph) and G_{Ca} (lower graph) normalized to their peak values measured from the model during the ascending phase of the ramp voltage-clamp command at different levels of synaptic excitation. The horizontal and vertical dashed lines show the graded decrease in the PIC somatic activation threshold and graded increase in the amplitude of Ca^{2+} PIC, respectively, as more synapses are activated. a, b, c and d are as defined in Fig. 2*A*. *C*, the change in magnitude of G_{Ca} with respect to synaptic current at different membrane potentials (–50 to –70 mV) under voltage-clamp conditions in *B*.

© 2006 The Authors. Journal compilation © 2006 The Physiological Society

(Fig. 5*F*, circles). This all-or-none activation of the Ca^{2+} PIC occurred exactly upon cell recruitment (compare Fig. 5*F* to Fig. 6*B* where cell recruitment took place at 5 nA). These results demonstrate that the AHP serves a critical role in maintaining (clamping) the membrane potential below the firing level, and preventing the Ca^{2+} PIC from being activated in an all-or-none manner. The conductance of the dendritic $Ca_v1.3$ channels (G_{Ca}) is voltage dependent. Therefore, the induced reduction in membrane potential during the AHP reduces G_{Ca}, hence, limiting the activation of the Ca^{2+} PIC. On the other hand, the increase in spike threshold with firing allows gradual activation of the Ca^{2+} PIC until it eventually reaches its saturation level (not illustrated).

To further investigate the mode of activation of the Ca^{2+} PIC during normal firing behaviour, the input–output *F–I* relationship (synaptic *F–I* relationship) was obtained by plotting the steady-state firing rate responses of Fig. 4*A* against the effective synaptic current (hyperpolarized Ia I_N; Fig. 6*A*) and compared to the dendritic G_{Ca} profile (Fig. 6*B*). Prior to cell recruitment, the dendritic G_{Ca} gradually increased with increasing synaptic input (Fig. 6*B*). Acceleration in the rate of increase in G_{Ca} with synaptic current was seen just before recruitment reflecting the increase in magnitude of the Ca^{2+} PIC relative to that of the leak current in the voltage range before the NSR on the *I–V* relationship (Fig. 2*C*). Upon the onset of cell firing, the rate of increase of G_{Ca} was abruptly decreased (notch in Fig. 6*B*) due to the clamping effect of the AHP. This effect of the AHP prevented an all-or-none jump in the magnitude of G_{Ca} (as shown in Fig. 5*F*, circles) and instead forced the G_{Ca} (dendritic Ca^{2+} PIC) to be graded with increasing synaptic input (region denoted by s in Fig. 6*B*). This graded increase in the Ca^{2+} PIC in response to incremental increases in the effective synaptic current resulted in a relatively steep increase in the firing rate (gain = 6 impulses s^{-1} nA^{-1}), coinciding with what is classically termed the secondary range of the *F–I* relation (denoted by s in Fig. 6*A*; Kernell, 1965*a*,*b*). Additional synaptic input caused the G_{Ca} to saturate near its maximal value leading to full activation of the dendritic Ca^{2+} PIC (region denoted by t in Fig. 6*B*). Because of the saturated Ca^{2+} PIC, the firing rate increased more slowly with increasing synaptic current in the region classically termed the tertiary range of the *F–I* relationship (slope 2.6 impulses s^{-1} nA^{-1}; denoted by t range of Fig. 6*A*). The tertiary range had a lower gain (slope) both because of the lack of increase in the Ca^{2+} PIC, and because the added conductance of the $Ca_v1.3$ channels resulted in a reduction in the cell input resistance, thus additional synaptic input produced a smaller increase in firing rate. This firing behaviour (synaptic *F–I* relation) closely matches that seen experimentally in spinal motoneurones when activated synaptically as opposed to being activated through intracellular current injection (Fig. 7 in Heckman *et al.* 2005).

In summary, during normal firing behaviour, an increasing synaptic input initially activates the Ca^{2+} PIC in a graded manner, followed by a saturation range in which the Ca^{2+} PIC is fully activated. These distinct modes of activation lead to the secondary and tertiary firing ranges, respectively, in the synaptic *F–I* relationship. Due to the clamping of the membrane potential by the AHP during cell firing, no all-or-none activation of the Ca^{2+} PIC takes place.

Intracellular *versus* synaptic activation

The activation of the Ca^{2+} PIC was compared during somatic intracellular current injection to that during synaptic activation. In Fig. 7*A*, the *F–I* relationship was obtained under two conditions: intracellular injection of a slow triangular current ramp at the soma (triangles), and synaptic activation (circles). The level of activation of the $Ca_v1.3$ channels during these conditions is expressed by the G_{Ca} profile in Fig. 7*B*. With intracellular current injection, the *F–I* relationship exhibited the three classical ranges of firing rates: primary, secondary, and a tertiary range. In the primary range (denoted by p in Fig. 7*A* and *B*), there was low activation of the Ca^{2+} PIC indicated by the low magnitude of G_{Ca} in Fig. 7*B*. Further current injection gradually activated the Ca^{2+} PIC, indicated by the increased level of G_{Ca} in the secondary range (denoted by s with triangles in Fig. 7*A* and *B*). This increased activation of the Ca^{2+} PIC lead to the steep increase in cell firing seen during the secondary range of the *F–I* relationship. At higher levels of current injection, Ca^{2+} PIC was fully activated, indicated by the saturation in G_{Ca}, during the tertiary range (denoted by t with triangles in Fig. 7*A* and *B*). Saturation of the Ca^{2+} PIC resulted in the reduced firing rate seen during the tertiary range of the *F–I* relationship. In contrast, with synaptic activation, the *F–I* relationship exhibited only secondary and tertiary ranges (denoted by s and t with circles in Fig. 7*A* and *B*). The Ca^{2+} PIC was always activated before cell recruitment, thus no primary range was seen in the synaptic *F–I* relationship. Note that the slight mismatch between the firing behaviour and G_{Ca} (in Fig. 7*A* and *B*) is due to the fact that only one synaptic input (Ia-afferent system) is represented in the model. Activation of the $Ca_v1.3$ channels is proportional to the proximity of these channels to the Ia-synapses. Given that the depolarization provided by this system is inadequate to activate all the $Ca_v1.3$ channels, the average G_{Ca} underestimates the conductance of those channels actually activated by the synaptic input and results in the seen mismatch.

The threshold for activating plateau potentials with somatic intracellular current injection was compared to that with synaptic excitation. Plateau potentials were activated at lower current and voltage thresholds with

© 2006 The Authors. Journal compilation © 2006 The Physiological Society

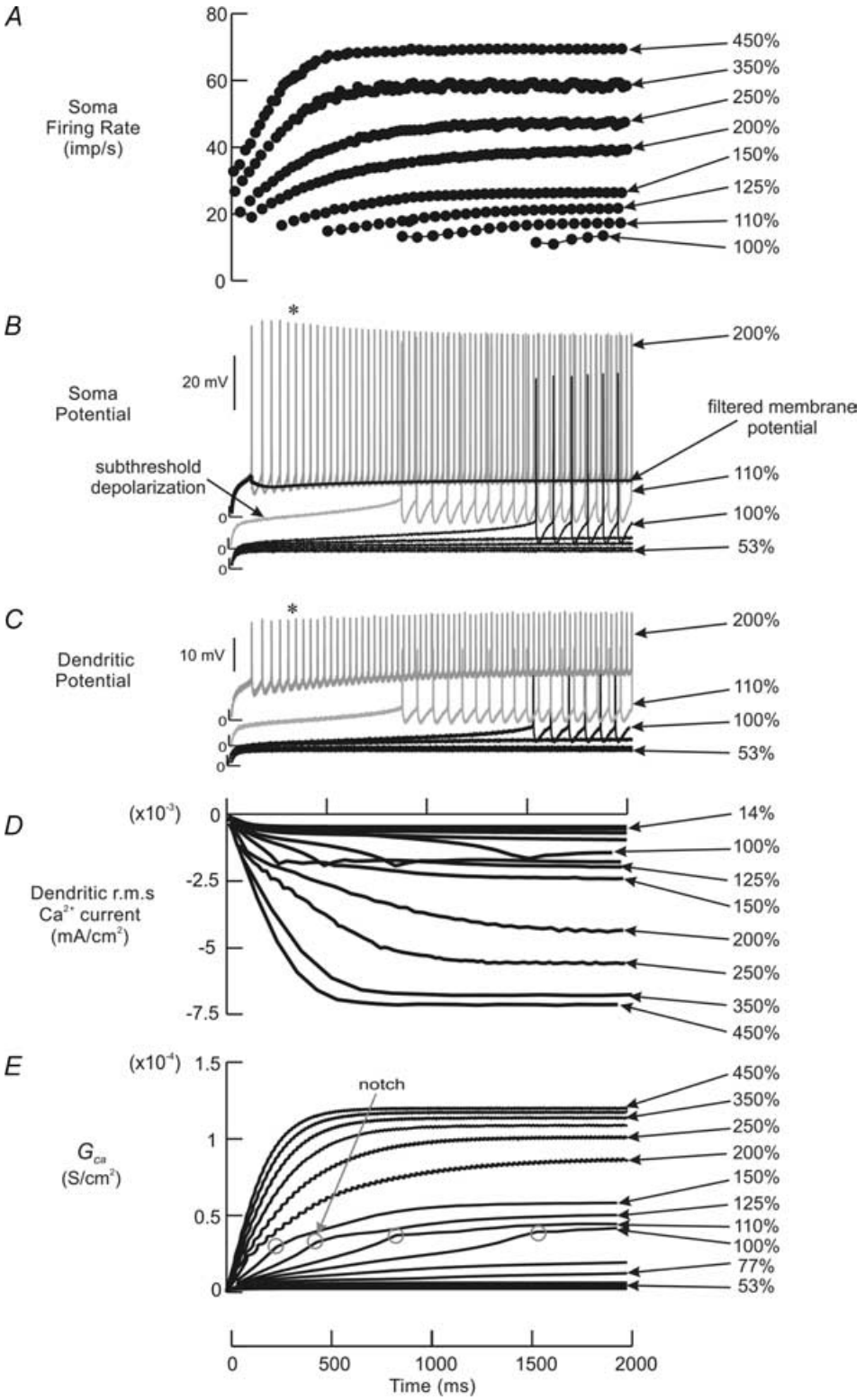

Figure 4. Measurements from the soma and a dendritic compartment during cell firing at different levels of synaptic excitation

For each level of synaptic excitation, the recordings show the soma firing rate (impulses s^{-1}; *A*), soma spikes (*B*), dendritic spikes measured from a dendritic compartment located at 695.9 μm (0.52 λ) from the soma (*C*), dendritic

© 2006 The Authors. Journal compilation © 2006 The Physiological Society

synaptic excitation alone than with intracellular current injection alone. Synaptic excitation that provided an effective synaptic current of 5.4 nA was able to activate plateau potentials, while a somatic intracellular long current pulse of 8 nA was needed to activate them (compare the vertical dashed line in Fig. 2*B* to that in Fig. 7*C*). Furthermore, the somatic voltage threshold at which plateau potentials were activated by synaptic excitation alone (−60 mV) was lower than that with intracellular current injection alone (−56 mV; compare the horizontal dashed line in Fig. 2*B* to that in Fig. 7*C*).

Enhancement of synaptic current

Enhancement of synaptic current by the added PIC and its resultant effect on the motoneurone firing rate was previously investigated in many studies; however, discrepancies in reports between variable (Hultborn *et al.* 2003) and constant (Prather *et al.* 2001) enhancement of synaptic current are seen. In this section, we examined enhancement of synaptic current by the Ca^{2+} PIC, and explained it based on the distinct modes of activation of the Ca^{2+} PIC. Simulations were run under voltage-clamp conditions at different levels of synaptic excitation. For each level of steady Ia-synaptic excitation, the synaptic current was computed as the difference between the *I–V* relationships during no synaptic activity and during synaptic excitation (Lee & Heckman, 2000). The hyperpolarized Ia I_N represented the synaptic input unaugmented by the Ca^{2+} PIC, whereas the peak Ia I_N included the activation of the Ca^{2+} PIC and the hyperpolarized Ia I_N (Fig. 6*C*). The difference between the peak Ia I_N and hyperpolarized Ia I_N represented the amount of augmentation in synaptic current (synaptic enhancement) caused by the activation of the Ca^{2+} PIC at different levels of synaptic excitation (Fig. 6*D*). Before cell recruitment, the Ca^{2+} PIC was activated in a graded manner and resulted in a linear enhancement of synaptic current in proportion to the level of synaptic excitation (from 14 to 100% of synaptic excitation; slope = 1.3, $r^2 = 0.97$ for the left regression line in Fig. 6*D*). Upon cell recruitment, activation of the Ca^{2+} PIC was limited by the clamping effect of the AHP and resulted in a shallower linear enhancement of synaptic current during the secondary range of the synaptic *F–I* relationship (from 100 to 200% of synaptic excitation; slope = 0.26, $r^2 = 0.96$ for the middle regression line in Fig. 6*D*). During the tertiary range, the Ca^{2+} PIC was saturated and resulted in a constant enhancement of synaptic current (for synaptic excitation > 200%; slope = –0.016, $r^2 = 0.33$ for the right regression line in Fig. 6*D*).

Summation of synaptic inputs

Activation of the Ca^{2+} PIC by multiple synaptic inputs and its effect on summation of these inputs was also investigated. The cell was initially activated with a bias current to achieve a low background firing level. Two additional test synaptic inputs (A and B) with incremental strengths were then applied and changes in firing rate relative to the background firing rate were computed. The change in steady-state firing rate evoked from the concurrent activation of the two test synaptic inputs (A & B) was compared to the linear sum of changes in steady-state firing rates evoked from the individual activation of each test synaptic input (A + B). Two different methods were used to activate the cell to provide background cell firing: synaptic activation (Fig. 8*A*), and intracellular current injection at the soma (Fig. 8*D*). Figure 8*B* shows the *F–I* relationship obtained by simultaneous application of the synaptic bias current and the two test synaptic inputs, and Fig. 8*C* compares the changes in firing rate evoked by the concurrent activation of the two test synaptic inputs to the linear sum of their individual changes in firing rate. When the test synaptic inputs A and B individually caused the cell to fire in the secondary range, and their concurrent activation caused the cell to also fire in the secondary range (conditions 1 and 2 in Fig. 8*B*), summation of synaptic inputs was nearly equal to their linear sum (Fig. 8*C*; condition 1 & 2). When either test synaptic input A or B caused the cell to fire in the secondary range, but their concurrent activation caused the cell to fire in the tertiary range (conditions 2 and 3 in Fig. 8*B*), or when the test synaptic inputs A and B individually caused the cell to fire in the tertiary range (conditions 4 and 5 in Fig. 8*B*), summation of synaptic inputs was less than their linear sum (Fig. 8*C*; conditions 2 & 3 and 4 & 5). Less-than linear summation resulted from the full activation of the Ca^{2+} PIC leading to a tertiary range of shallower gain. Therefore, linear summation is seen at moderate firing rates that correspond to the range of graded activation of the Ca^{2+} PIC, whereas less-than linear summation is seen at relatively high firing rates that correspond to the saturation of the Ca^{2+} PIC.

Given that it is often difficult experimentally to induce a cell to fire throughout its range of firing with synaptic inputs alone, intracellular current injection at the soma was the experimentally used method for obtaining the

root mean square Ca^{2+} current measured from the same dendritic compartment (*D*), G_{Ca} (*E*). * Traces are shifted up for clearer display and avoidance of overlap. Grey circles (notches) show the abrupt change in G_{Ca} upon firing onset. Thick black line in *B* shows the filtered somatic membrane potential during cell firing.

© 2006 The Authors. Journal compilation © 2006 The Physiological Society

background firing in studying synaptic summation in real motoneurones (e.g. Powers & Binder, 2000; Prather *et al.* 2001). We thus also simulated this approach by injecting an intracellular bias current at the soma, followed by activation of the test synaptic inputs (Fig. 8*D*). With somatically injected bias current, the *F–I* relationship obtained from subsequent synaptic inputs was shifted to the right. More importantly the firing ranges were shifted upwards (secondary range occurred at higher rates) due to the greater difficulty in activating PICs from the soma compared to the dendrites, and a primary range emerged (Fig. 8*E*) as a by-product of this intracellular current injection. When either test synaptic input A or B was weak relative to the bias current thus causing the cell to fire in its

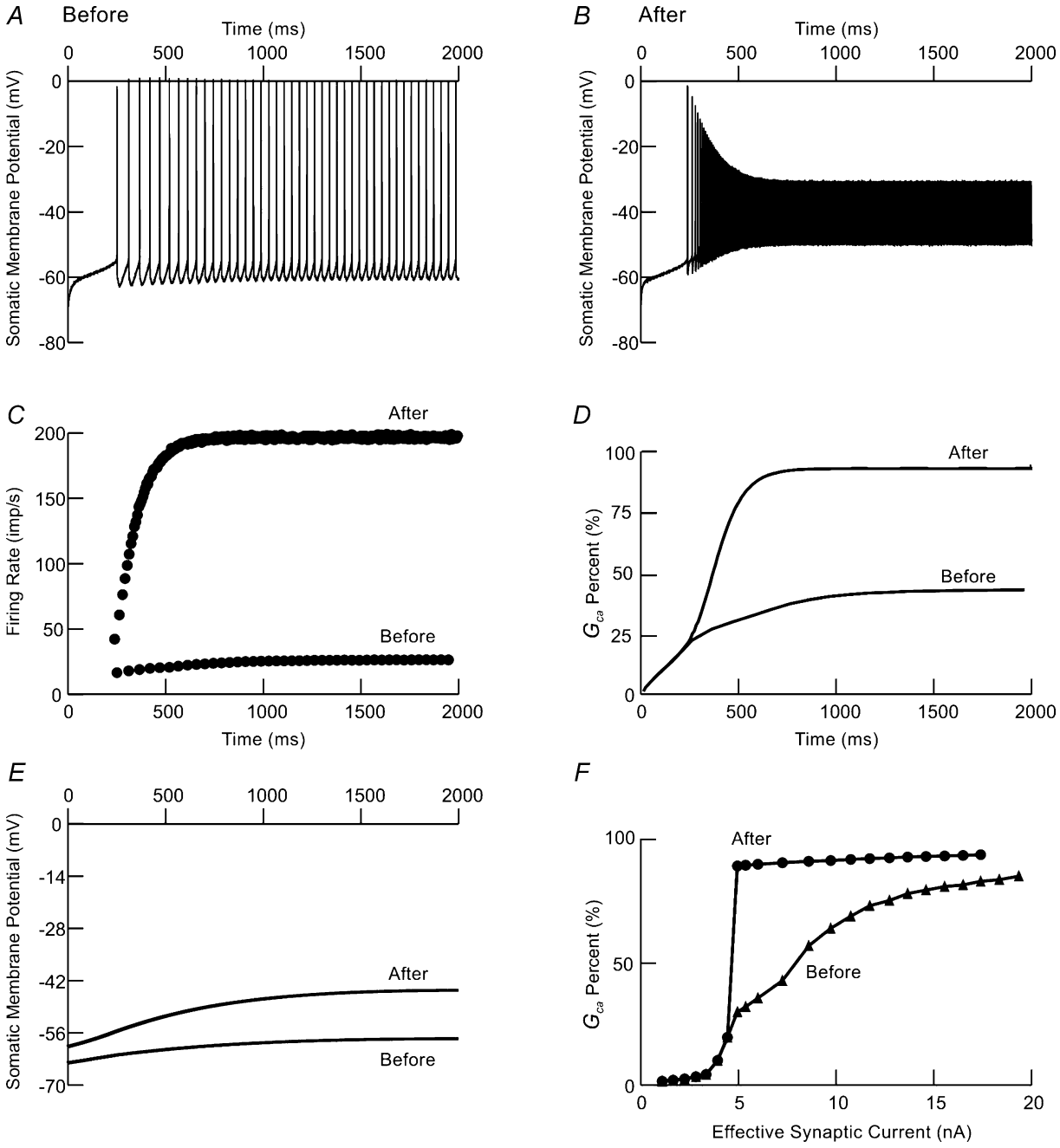

Figure 5. Effect of the AHP on activation of the Ca^{2+} PIC
Somatic spikes before (*A*) and after (*B*) blocking the K(Ca) channels, cell firing rate (*C*), relative magnitude of G_{Ca} (*D*), and the filtered somatic membrane potential (*E*) in response to 150% of synaptic excitation. *F*, the change in magnitude of G_{Ca} with respect to synaptic current before and after blocking the K(Ca) channels at different levels of synaptic excitation (from 14 to 400%).

© 2006 The Authors. Journal compilation © 2006 The Physiological Society

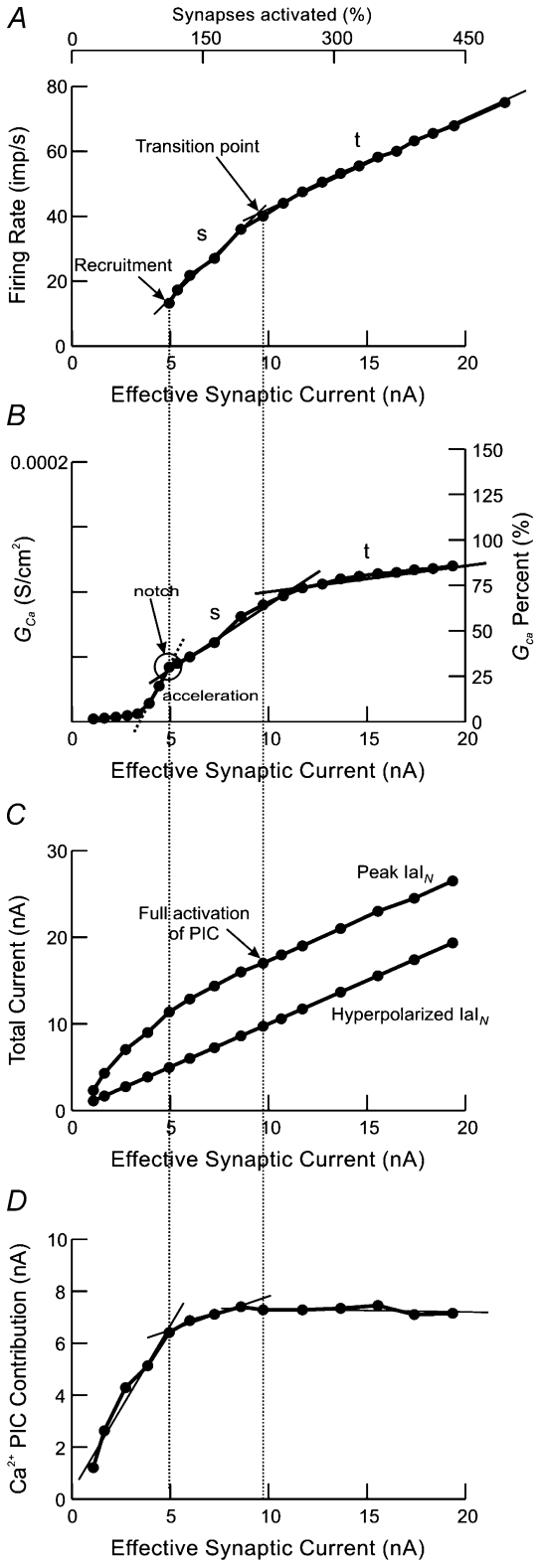

Figure 6. Mode of activation of Ca^{+2} PIC during normal firing and enhancement of synaptic current
A, steady-state *F–I* relationship evoked by synaptic excitation. The top axis shows the percentage of activated synapses at each level. Thin continuous lines: linear fits for secondary (s, $r^2 = 0.995$) and tertiary (t, $r^2 = 0.994$) segments. Transition point indicates change in slope between the secondary and tertiary segments. Long dashed vertical lines represent the point at which the cell is recruited and the point of full activation of Ca^{2+} PIC, respectively. The latter corresponds to the transition from the secondary to tertiary ranges on the synaptic *F–I* relationship. *B*, steady-state magnitude of G_{Ca} at different levels of synaptic excitation. Right axis shows the percentage increase in G_{Ca} relative to its maximum achievable value. Thin continuous lines: linear fits for increase in G_{Ca} in the secondary ($r^2 = 0.98$) and tertiary ($r^2 = 0.97$) ranges. Dashed line shows the acceleration in the magnitude of G_{Ca} during the period of graded activation of Ca^{2+} PIC. Circle (notch) shows the abrupt change in G_{Ca} upon firing onset. *C*, hyperpolarized and peak Ia I_N C, measurements from the model at different levels of synaptic excitation, indicated by the effective synaptic current at resting potential. At each level of synaptic excitation, the Ia I_N was computed as the difference between the *I–V* relationships during no synaptic activity and during tendon vibration at 180 Hz. *D*, contribution of Ca^{2+} PIC to the synaptic current at different levels of synaptic excitation. This was computed as the difference between the peak and hyperpolarized Ia I_N traces presented in *C* at each level of synaptic excitation. Thin lines: linear fits representing PIC contribution to the enhancement of synaptic current before recruitment (slope = 1.3, $r^2 = 0.97$), during the secondary range (slope = 0.26, $r^2 = 0.96$), and during the tertiary range (slope = –0.016, $r^2 = 0.33$).

primary range, but the concurrent activation of A and B caused the cell to fire in the secondary range (conditions 1 and 2 in Fig. 8*E*), summation of synaptic inputs was greater than their linear sum. However, during the secondary and tertiary firing ranges of the *F–I* relationship, linear and less-than linear summation occurred, respectively (Fig. 8*E*). In Fig. 8*F*, greater-than linear summation is seen at relatively low firing rates that correspond to the range before activation of the Ca^{2+} PIC, whereas less-than linear summation is seen at relatively high firing rates that correspond to the saturation of the Ca^{2+} PIC. Similar results were obtained when different magnitudes (10 and 12 nA) of intracellular bias current were used (Fig. 8*F*, filled circles and open squares, respectively).

Discussion

Model predicts that dendritic PIC has a graded followed by saturated activation with increasing synaptic current

Discrepancies in experimental reports regarding the behaviour of PICs make it difficult to infer their mode of activation and whether it is graded or all-or-none (see Hultborn *et al.* 2003; Lee *et al.* 2003). Disparities in the role of PICs in the enhancement and summation of synaptic inputs are also reported (Powers & Binder, 2000; Prather *et al.* 2001; Hultborn *et al.* 2003). However, direct measurements of the dendritic PIC during synaptically evoked firing to resolve these discrepancies, as we have done with our simulations, is experimentally unfeasible in real motoneurones for the following reasons: (1) it is difficult to record directly from the very small and extensive dendrites of a motoneurone; (2) it is difficult to

© 2006 The Authors. Journal compilation © 2006 The Physiological Society

activate sufficient numbers of synaptic inputs to activate the cell fully; and (3) the net Ca^{2+} PIC seen at the soma, which is feasible to measure under voltage clamp, cannot be measured during natural cell firing. Thus, computer simulations were used in the present study to examine the mode of activation of the dendritic Ca^{2+} PIC during cell firing, and to elucidate its role in the enhancement and summation of synaptic inputs. Our modelling results suggest that under physiological conditions (i.e. when the cell is free to fire) an increasing synaptic input does *not* lead to an all-or-none activation of the dendritic Ca^{2+} PIC, even when steady-state responses to increasing synaptic steps are evaluated (Fig. 6*B*). Instead, the level of activation of the dendritic Ca^{2+} PIC is initially graded with increasing synaptic input until it reaches its saturation level, after which further increases in synaptic input cause minimal changes in the Ca^{2+} PIC. The range of graded activation of the Ca^{2+} PIC corresponds to the secondary range of firing (in the synaptic *F–I* relationship), and the range of saturated activation of the Ca^{2+} PIC corresponds to the tertiary range of firing. The results of our simulations provided an explanation for the process of dendritic Ca^{2+} PIC activation during cell firing. It also helped in resolving the discrepancies in previous experimental reports regarding the enhancement and integration of synaptic inputs, as described below.

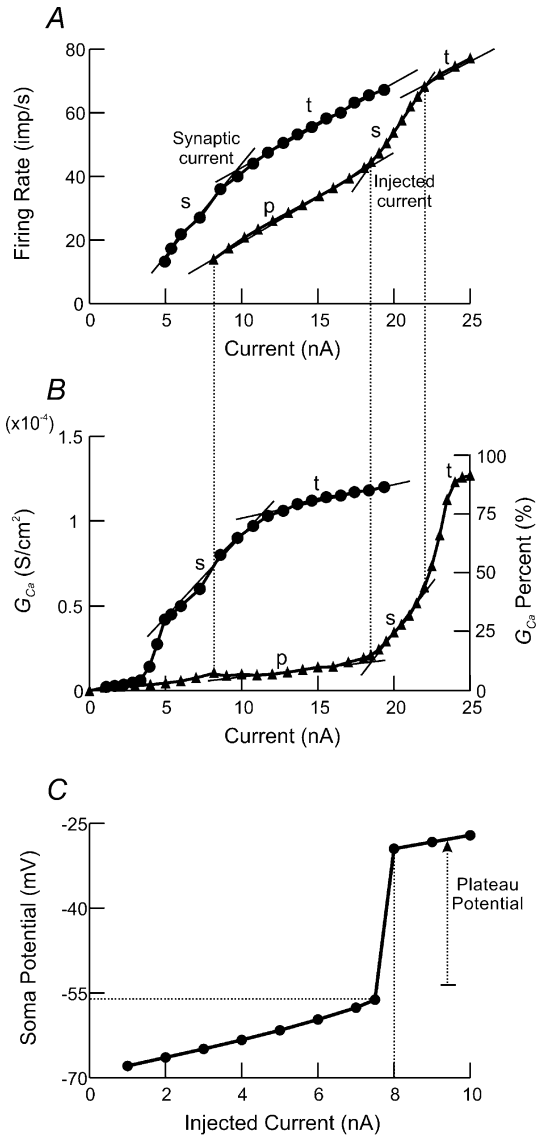

Figure 7. Comparison of the efficacy of intracellular current injection in activating the PIC to that of synaptic excitation
A, comparison of *F–I* relationships evoked by synaptic activation (circles) and intracellular current injection (triangles) at the soma. *B*, steady-state magnitude of G_{Ca} measured for the *F–I* relationships in *A*. Right axis shows the percentage increase in G_{Ca} relative to its maximum achievable value. *C*, steady-state somatic membrane potential in response to intracellular long current pulses injected at the soma. Horizontal dashed line shows the somatic plateau threshold (–56 mV). Vertical dashed line shows the current level at which the somatic plateau threshold takes place (8 nA).

Previous experimental measurements from rat motoneurones suggest that the secondary and tertiary ranges of firing are indeed caused by the dendritic Ca^{2+} PIC since these ranges are eliminated when the LVA L-type Ca^{2+} channels are blocked by nimodipine, leaving only a primary range (Li *et al.* 2004; Heckman *et al.* 2005). The graded activation of the Ca^{2+} PIC in the secondary range, as opposed to an all-or-none Ca^{2+} PIC activation, occurs as a result of the AHP forcing (effectively clamping) the membrane potential to remain below the firing level throughout the interspike interval. The AHP's effect on limiting the activation of the PIC has been previously proposed (Hounsgaard & Mintz, 1988; Li *et al.* 2004), but was directly confirmed in the present study by demonstrating that the all-or-none activation of the Ca^{2+} PIC for an increasing synaptic input occurs when the K(Ca) channels mediating the AHP are blocked (Fig. 5) or when the spikes are themselves blocked (Fig. 2; compare to the QX-314 data of Lee & Heckman, 1999, in cat motoneurones, the TTX data of Hounsgaard & Kiehn, 1989, in turtle motoneurones, and Li & Bennett, 2003, in rat motoneurones). The role of the AHP in limiting the activation of the PIC could be confirmed experimentally by examining the effect of apamin (a specific small conductance K^+ channel blocker) on cell firing during current clamp. Furthermore, a similar graded activation of the Ca^{2+} PIC occurs when the motoneurone is voltage-clamped (Fig. 3; also similar to voltage-clamp data of Lee & Heckman, 1998*b*, in cat motoneurones, Svirskis & Hounsgaard, 1998, in turtle motoneurones, and Li & Bennett, 2003, in rat motoneurones). Because the firing threshold gradually increases with firing rate (Schwindt & Crill, 1982), the PIC becomes gradually activated as the firing rate increases in the secondary range until saturation is reached (tertiary range).

© 2006 The Authors. Journal compilation © 2006 The Physiological Society

Experimental data supporting graded Ca^{2+} PIC activation followed by saturation

We re-examined previously published *experimental* data for rat motoneurones during current- and voltage-clamp experiments to verify the activation ranges of the Ca^{2+} PIC (data adapted from Fig. 2*B* and *C* in Li *et al.* 2004). The average somatic membrane potential during firing was used as the common factor for relating the experimentally measured firing rate evoked during current clamp to the Ca^{2+} PIC measured during the voltage-clamp experiment (Fig. 9). During the ascending segment of the current ramp command, the primary range of cell firing was found to correspond to the range preceding the activation of the Ca^{2+} PIC (left range 1 in Fig. 9). During the secondary range of cell firing, the Ca^{2+} PIC corresponded to the NSR of the *I–V* relationship (left range 2 in Fig. 9). Activation of the Ca^{2+} PIC was graded in this region because the slope of the *F–I* relationship, though relatively steep, was far from vertical. Increasing current caused an increase in firing rate, further depolarization of the cell membrane and further activation of the Ca^{2+} PIC (grading). The graded or partial activation of the Ca^{2+} PIC within this range is probably due to the clamping effect of the AHP described earlier. The tertiary range, on the other hand, corresponded to the range during which the Ca^{2+} PIC was fully activated (left range 3 in Fig. 9), and minimal PIC grading took place in this range. The tertiary range was maintained until the cell was nearly de-recruited on the descending segment of the current ramp command (right range 3 in Fig. 9) due to the hysteresis in the Ca^{2+} PIC. Thus, it is interesting to note that *no PIC grading* occurs through most of the range of firing frequencies during the down voltage ramp.

The finding that Ca^{2+} PIC can be graded, for at least a short duration following cell recruitment (in the secondary range; Fig. 6*A* and *B*), has additional support in a number of experimental observations which are summarized as follows. (1) Graded synaptic activation provided by muscle stretch causes a gradual increase in firing rate. This is then followed by a shallower tertiary range during which firing rate increases only slightly with synaptic current (Lee *et al.* 2003; Heckman *et al.* 2005). (2) The steady-state firing of the secondary range has been shown to be mediated by the activation of the Ca^{2+} PIC in motoneurones (Schwindt & Crill, 1982; Li *et al.* 2004). Moreover, Kernell (1965*b*) and Schwindt & Crill (1982) have shown that steady-state firing is possible in the middle of the secondary range; thus, stable partial activation of the Ca^{2+} PIC is obtainable, consistent with the concept of graded activation of the Ca^{2+} PIC in this range. (3) Voltage-dependent enhancement of synaptic current is found to be a smooth function of the holding potential (Lee & Heckman, 2000). (4) Under voltage-clamp conditions, stretch-evoked synaptic current is usually graded despite the rapid acceleration in firing rate sometimes seen under unclamped conditions (Lee *et al.* 2003). (5) Synaptic input provided by muscle stretch causes a graded increase in firing rate prior to saturation (Lee *et al.* 2003). (6) Graded (variable) amplification of firing rates is seen in decerebrate cat motoneurones in response to brief intermittent synaptic activation (Hultborn *et al.* 2003). Conversely, all-or-none activation of plateau potentials seen in current-clamp experiments when the spikes are blocked is probably due to the absence of the AHP, which limits the activation of the PIC as shown in the present study (Fig. 2).

Previous experimental recordings from human motor units also support an initially graded PIC activation followed by saturation. During increasing contractions, recordings from high threshold motor units (Romaiguere *et al.* 1989) showed a steep increase in firing rate after recruitment, in what appeared to be a fairly long and stable secondary range of firing (as in our Fig. 6*A*). Following this, further increases in contraction produced a lesser increase in firing rate, in what appeared to be the shallower tertiary range. This behaviour is consistent with the graded activation of the Ca^{2+} PIC in the secondary range, followed by its saturation in the tertiary range, as seen from the simulations in the present study.

Exceptions, where all-or-none PIC activation may occur

In low threshold human motor units (Romaiguere *et al.* 1989; Gorassini *et al.* 2002) as well as in many rat motor units (Bennett *et al.* 2001), firing accelerates only over the first few spikes after recruitment, if at all, during a slowly increasing contraction. Following that, the firing rate increases slowly in what appears to be the tertiary range. The brief acceleration in firing at recruitment does not vary with the speed of the synaptic input (or rate of rise of contraction as in Romaiguere *et al.* 1989), and is thus probably due to the subthreshold activation of a large Ca^{2+} PIC in an all-or-none manner due to the absence of the AHP. Shortly after cell recruitment the Ca^{2+} PIC is saturated, and firing occurs in the tertiary range. A similar behaviour in which cells fire in their tertiary range shortly after recruitment is also seen in many rat motoneurones when activated with intracellular current injection (Li *et al.* 2004). No extensive secondary range occurs in these cells because the Ca^{2+} PIC is mostly activated at recruitment; however, the Ca^{2+} PIC still helps in recruiting these cells and maintaining firing (enabling self-sustained firing; Li *et al.* 2004).

Although unusual, some cat motoneurones occasionally have an abrupt increase in firing rate in response to muscle stretch that occurs somewhat *after* recruitment, unlike the motoneurones just described (Hounsgaard *et al.* 1988; Lee *et al.* 2003). This behaviour appears to be unstable as it

© 2006 The Authors. Journal compilation © 2006 The Physiological Society

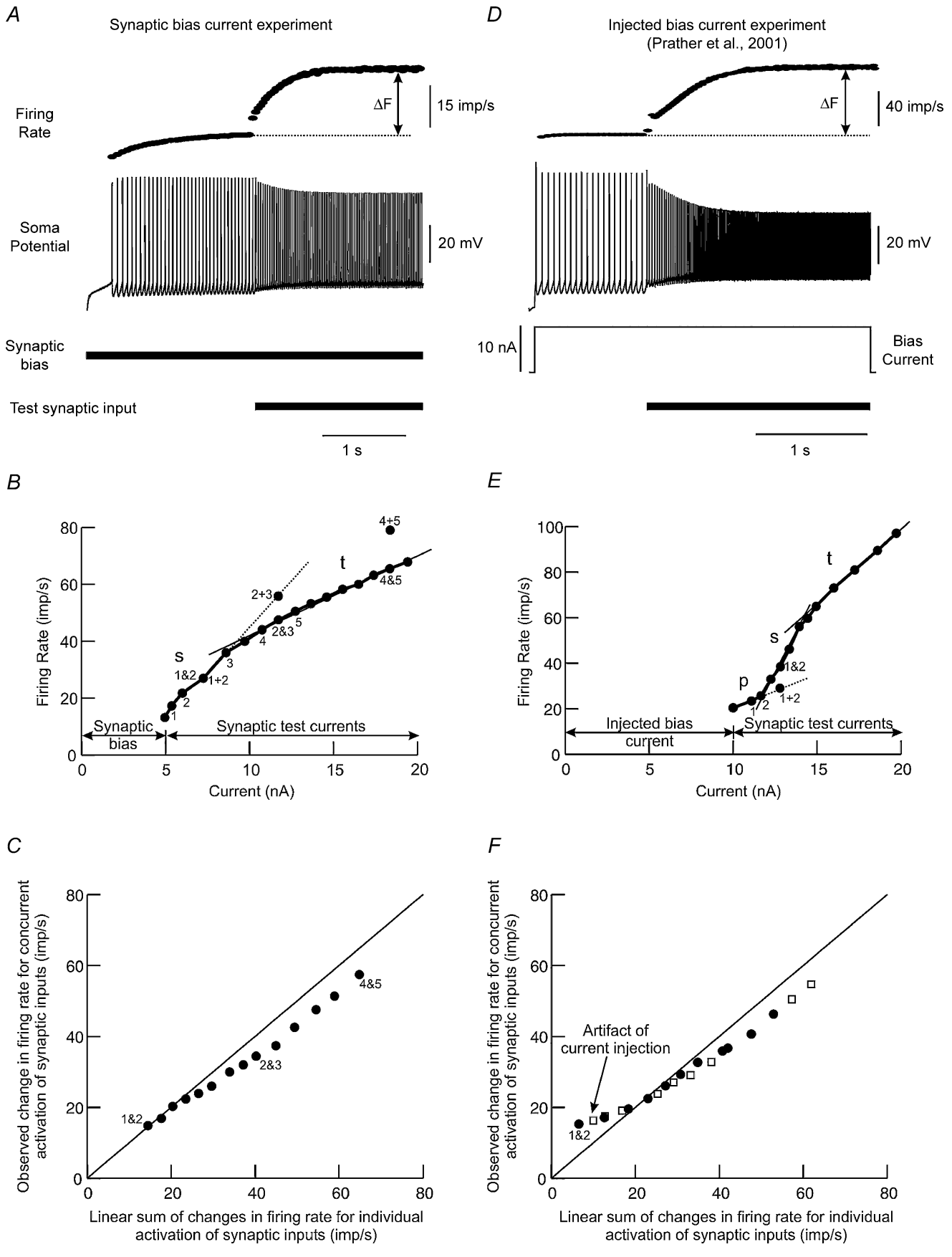

© 2006 The Authors. Journal compilation © 2006 The Physiological Society

occurs only on some stretches, and suggests an all-or-none activation of the PIC during cell firing (Lee *et al.* 2003). If this were the case, the magnitude of the Ca^{2+} PIC must be very large in these motoneurones and activated in distal dendritic regions that are not easily affected by the clamping effect of the AHP associated with cell firing.

Enhancement of synaptic current

Previous experimental and modelling studies showed that the amount of synaptic current from various presynaptic systems is inadequate to cause the cell firing levels seen during natural motor activity (Powers & Binder, 1995, 2001; Rose & Cushing, 1999). Later, it was shown experimentally that activation of PICs enhances the synaptic input to motoneurones and results in the observed amplified firing behaviour (Bennett *et al.* 1998; Lee & Heckman, 2000; Prather *et al.* 2001; Hultborn *et al.* 2003; Lee *et al.* 2003). Our simulations suggest that during the graded activation of the Ca^{2+} PIC, the enhancement of synaptic input is linearly graded in proportion to the level of synaptic excitation, whereas following the saturation of the Ca^{2+} PIC, the enhancement of synaptic input is constant.

These results could provide an explanation for the discrepancy in reports regarding the magnitude of enhancement of synaptic currents by Ca^{2+} PIC. In a study by Hultborn *et al.* (2003) experimental recordings obtained from decerebrate cat motoneurones showed graded (variable) enhancement of synaptic inputs as the PIC was activated. This graded enhancement of synaptic inputs may be due to the relatively small injected and synaptic inputs used to activate the cell, and could have resulted in partial activation of the PIC causing the cell to fire in the secondary range of the *F–I* relationship. This is comparable to the range of graded Ca^{2+} PIC activation that shows linear enhancement of synaptic inputs in our results. In contrast, Prather *et al.* (2001) reported constant enhancement of synaptic inputs by the PIC (indicated by a vertical shift in the *F–I* relationship relative to that predicted when the synaptic input was applied) also from decerebrate cat motoneurones. The constant enhancement of synaptic inputs may be due to the relatively high current injections (up to 40 nA) used to activate the motoneurones in that study, which result in full activation of the PIC and cause the cell to fire mostly in the tertiary range of the *F–I* relationship. This is comparable to the range of saturated Ca^{2+} PIC activation that shows constant enhancement of synaptic inputs in the present study.

Intracellular *versus* synaptic activation

Our simulations demonstrate that motoneurone activation through synaptic excitation is different from that seen through somatic current injection, which has also been shown in previous studies (Kernell, 1965*c*; Shapovalov, 1972; Brownstone *et al.* 1992; Bennett *et al.* 1998). Synaptic excitation is more efficient in exciting the motoneurone and triggering the plateau potentials than intracellular current injection. With synaptic excitation, membrane depolarization is initiated in the dendritic tree where the $Ca_v1.3$ channels are located, and then spreads to the soma and initial segment and causes the cell to fire. Somatic current injection, on the other hand, initiates the membrane depolarization at the soma and directly triggers cell firing without PIC activation (Fig. 7*B* and *C*). Membrane depolarization then spreads from the soma to the dendritic tree opposite to the natural mode of activating motoneurones. Therefore, a primary range of firing with little Ca^{2+} PIC activation is seen in the current injected *F–I* relationship (Heckman *et al.* 2005). This primary range is a by-product of injecting current into the soma (Bennett *et al.* 1998; Heckman *et al.* 2005).

Summation of synaptic inputs

Our modelling results can also provide an explanation for the discrepancy in reports regarding the summation of synaptic inputs in motoneurones in which greater-than (Powers & Binder, 2000), less-than (Kuno & Miyahara, 1969) and linear summation (Burke, 1967; Prather *et al.*

Figure 8. Summation of synaptic inputs investigated when using synaptic (*A–C*) and injected (*D–F*) bias currents

Measurement of change in firing rate evoked by activating one of the two test synaptic inputs when synaptic (*A*) and injected (*D*) bias currents were used. Change in firing rate (ΔF) was computed as the difference between steady-state firing rates before and after activation of the test synaptic input. In *D*, a bias current of 10 nA was used to obtain background firing. Steady-state synaptic *F–I* relationships evoked from simultaneous application of the bias current and the test synaptic input when synaptic (*B*) and injected (*E*) bias currents were used. Dashed lines in *B* and *E* represent extrapolation lines to the primary and secondary segments. 1 & 2 represents the change in firing rate evoked by *simultaneous* activation of the two test synaptic inputs, whereas 1 + 2 represents the linear sum of changes in firing rate evoked by *individual* activation of the test synaptic inputs represented by points 1 and 2. Comparison of changes in firing rate evoked by concurrent activation of the two test synaptic inputs and the linear sum of their individual changes in firing rate when synaptic (*C*) and injected (*F*) bias currents were used. Continuous line represents the line of unity at which the observed firing rate is equal to the linear sum. Data presented in *F* were obtained with injected bias current of 10 nA (●) and 12 nA (□).

© 2006 The Authors. Journal compilation © 2006 The Physiological Society

2001) are reported. Our results suggest that under physiological conditions, in which the motoneurone is activated synaptically, no greater-than linear summation takes place. Instead, linear summation of synaptic inputs occurs during the graded phase of the Ca^{2+} PIC (during the secondary range of the *F–I* relationship), and less-than linear summation occurs during the saturation phase of the Ca^{2+} PIC (during the tertiary range of the *F–I* relationship). Linear summation results from the existence of stable partial activation states of the PIC, while less-than linear summation results when the PIC is fully activated by synaptic inputs. We have shown that greater-than linear summation observed experimentally in previous studies (e.g. Powers & Binder, 2000; Prather *et al.* 2001) is probably due to using intracellular current injection in these experiments to produce background cell firing prior to applying the synaptic inputs. This somatic intracellular current enables the formation of a primary range of firing, not seen with synaptic input, and when subsequent synaptic inputs produce a transition of cell firing from the primary range to the secondary range greater-than linear summation occurs.

Model considerations

One could argue that saturation of the PIC is expected from a current whose steady-state activation is described by a Boltzmann function. Any ionic current that has no inactivation, like the Ca^{2+} PIC, will reach saturation when the membrane potential is sufficiently depolarized to have the underlying channels fully open. However, the question investigated in the present study is whether the PIC is activated in a graded or an all-or-none manner until it reaches its saturation level. We demonstrated that the graded activation of the Ca^{2+} PIC during cell firing is due to the clamping effect of the AHP on membrane potential. This was confirmed when an all-or-none activation of the Ca^{2+} PIC was seen during the blockade of the AHP either directly by blocking the K(Ca) channels (Fig. 5) or indirectly by blocking the spikes (Fig. 2). Moreover, the graded activation of the Ca^{2+} PIC had different slopes before and after the onset of cell firing, which cannot be described by a Boltzmann function (Fig. 6*B*).

In the present study we used a compartmental model for an FR motoneurone to study the mode of activation

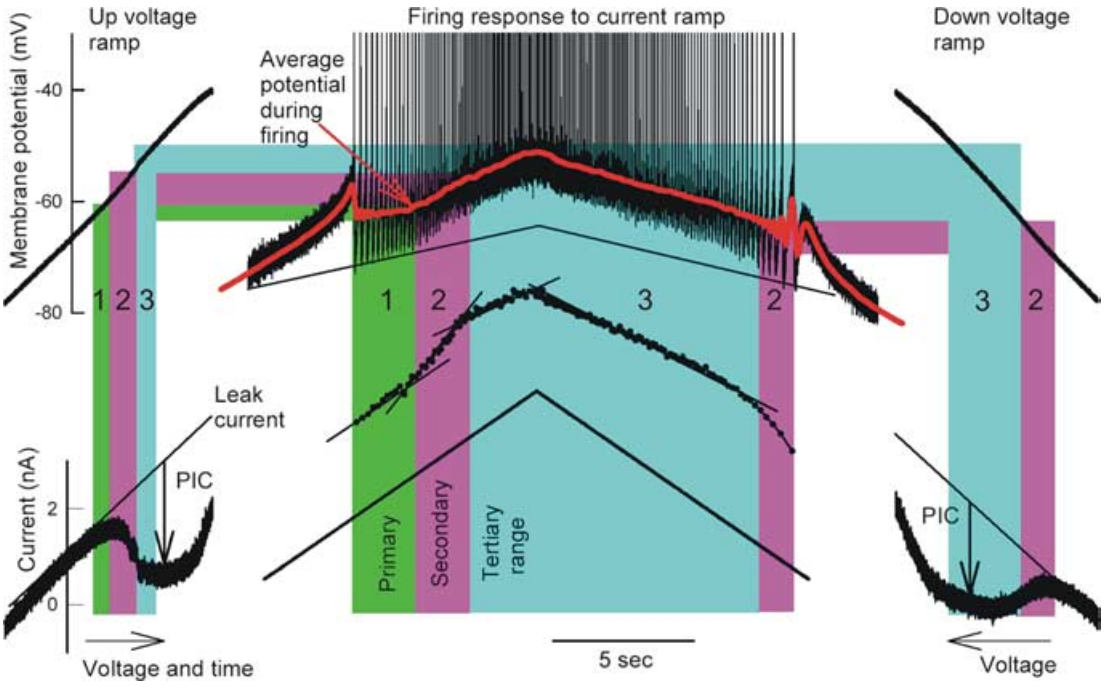

Figure 9. Graded activation of Ca^{2+} PIC in rat motoneurone
Overlay of the *experimentally measured* firing rate (centre) and Ca^{2+} PIC (both sides) during ascending and descending ramp current- and voltage-clamp experiments, respectively, from a real rat motoneurone (data adapted from Fig. 2*B* and *C* in Li *et al.* 2004). The regions were marked as the primary, secondary and tertiary ranges of firing, and their corresponding locations on the *I–V* relationship were determined by using the filtered potential during firing (line labelled 'Average potential during firing'; 2 Hz low pass filter raw data) corresponding to the top and bottom of each range.

© 2006 The Authors. Journal compilation © 2006 The Physiological Society

of the dendritic Ca^{2+} PIC. However, our results could be extended to other types of motoneurones (S- and FF-types) and neuronal cells. A probable difference in S-type motoneurones is that the Ca^{2+} PIC will be activated at a lower threshold (Bennett *et al.* 1998) and the secondary range of cell firing with synaptic activation will be shorter.

Concluding remarks

In summary, computer simulations in the present study allowed direct assessment of the dendritic Ca^{2+} PIC during synaptically evoked cell firing. This helped in elucidating the nature of activation of the Ca^{2+} PIC and in resolving the discrepancies in previous reports regarding this question. It also allowed for the reconciliation of several conflicting experimental results on the role of PICs in the enhancement and integration of synaptic inputs.

References

Bennett DJ, Hultborn H, Fedirchuk B & Gorassini MA (1998). Synaptic activation of plateaus in hindlimb motoneurons of decerebrate cats. *J Neurophysiol* **80**, 2023–2037.

Bennett DJ, Li Y & Siu M (2001). Plateau potentials in sacrocaudal motoneurons of chronic spinal rats, recorded in vitro. *J Neurophysiol* **86**, 1955–1971.

Brannstrom T (1993). Quantitative synaptology of functionally different types of cat medial gastrocnemius alpha-motoneurons. *J Comp Neurol* **330**, 439–454.

Brownstone RM, Jordan LM, Kriellaars DJ, Noga BR & Shefchyk SJ (1992). On the regulation of repetitive firing in lumbar motoneurones during fictive locomotion in the cat. *Exp Brain Res* **90**, 441–455.

Burke RE (1967). Composite nature of the monosynaptic excitatory postsynaptic potential. *J Neurophysiol* **30**, 1114–1137.

Burke RE & Glenn LL (1996). Horseradish peroxidase study of the spatial and electrotonic distribution of group Ia synapses on type-identified ankle extensor motoneurons in the cat. *J Comp Neurol* **372**, 465–485.

Burke RE, Walmsley B & Hodgson JA (1979). HRP anatomy of group Ia afferent contacts on alpha motoneurones. *Brain Res* **160**, 347–352.

Cullheim S, Fleshman JW, Glenn LL & Burke RE (1987). Membrane area and dendritic structure in type-identified triceps surae alpha motoneurons. *J Comp Neurol* **255**, 68–81.

ElBasiouny SM, Bennett DJ & Mushahwar VK (2005*a*). Role of persistent inward currents (pics) in enhancement and integration of synaptic inputs in spinal motoneurons. *Abstract Viewer/Itinerary Planner, Society for Neuroscience, Washington, DC*. Online. Program no. 750.4.2005.

ElBasiouny SM, Bennett DJ & Mushahwar VK (2005*b*). Simulation of dendritic $Ca_v1.3$ channels in cat lumbar motoneurons: spatial distribution. *J Neurophysiol* **94**, 3961–3974.

ElBasiouny SM & Mushahwar VK (2004). Spatial distribution of low voltage-activated L-type calcium channels in the dendrites of cat lumbar motoneurons. *Abstract Viewer/Itinerary Planner, Society for Neuroscience, Washington, DC*. Online. Program no. 875.7.2004.

Fleshman JW, Segev I & Burke RE (1988). Electrotonic architecture of type-identified alpha-motoneurons in the cat spinal cord. *J Neurophysiol* **60**, 60–85.

Fyffe RE (1991). Spatial distribution of recurrent inhibitory synapses on spinal motoneurons in the cat. *J Neurophysiol* **65**, 1134–1149.

Glenn LL, Burke RE, Fleshman JW & Lev-Tov A (1982). Estimates of electrotonic distance of group Ia contacts on cat α-motoneurons: An HRP-morphological study. *Soc Neurosci Abstr* **8**, 995.

Gorassini MA, Yang JF, Siu M & Bennett DJ (2002). Intrinsic activation of human motoneurons: possible contribution to motor unit excitation. *J Neurophysiol* **87**, 1850–1858.

Granit R, Kernell D & Lamarre Y (1966*a*). Algebraical summation in synaptic activation of motoneurones firing within the 'primary range' to injected currents. *J Physiol* **187**, 379–399.

Granit R, Kernell D & Lamarre Y (1966*b*). Synaptic stimulation superimposed on motoneurones firing in the 'secondary range' to injected current. *J Physiol* **187**, 401–415.

Heckman CJ & Binder MD (1988). Analysis of effective synaptic currents generated by homonymous Ia afferent fibers in motoneurons of the cat. *J Neurophysiol* **60**, 1946–1966.

Heckman CJ, Gorassini MA & Bennett DJ (2005). Persistent inward currents in motoneuron dendrites: Implications for motor output. *Muscle Nerve* **31**, 135–156.

Hines M & Carnevale T (1997). The NEURON simulation environment. *Neural Comput* **9**, 1179–1209.

Hounsgaard J, Hultborn H, Jespersen B & Kiehn O (1988). Bistability of alpha-motoneurones in the decerebrate cat and in the acute spinal cat after intravenous 5-hydroxytryptophan. *J Physiol* **405**, 345–367.

Hounsgaard J & Kiehn O (1989). Serotonin-induced bistability of turtle motoneurones caused by a nifedipine-sensitive calcium plateau potential. *J Physiol* **414**, 265–282.

Hounsgaard J & Mintz I (1988). Calcium conductance and firing properties of spinal motoneurones in the turtle. *J Physiol* **398**, 591–603.

Hultborn H, Denton ME, Wienecke J & Nielsen JB (2003). Variable amplification of synaptic input to cat spinal motoneurones by dendritic persistent inward current. *J Physiol* **552**, 945–952.

Kernell D (1965*a*). The adaptation and the relation between discharge frequency and current strength of cat lumbosacral motoneurones stimulated by long-lasting injected currents. *Acta Physiol Scand* **65**, 65–73.

Kernell D (1965*b*). High-frequency repetitive firing of cat lumbosacral motoneurones stimulated by long-lasting injected currents. *Acta Physiol Scand* **65**, 74–86.

Kernell D (1965*c*). Synaptic influence on the repetitive activity elicited in cat lumbosacral motoneurones by long-lasting injected currents. *Acta Physiol Scand* **63**, 409–410.

Kuno M & Miyahara JT (1969). Non-linear summation of unit synaptic potentials in spinal motoneurones of the cat. *J Physiol* **201**, 465–477.

© 2006 The Authors. Journal compilation © 2006 The Physiological Society

Lee RH & Heckman CJ (1998*a*). Bistability in spinal motoneurons in vivo: systematic variations in rhythmic firing patterns. *J Neurophysiol* **80**, 572–582.

Lee RH & Heckman CJ (1998*b*). Bistability in spinal motoneurons in vivo: systematic variations in persistent inward currents. *J Neurophysiol* **80**, 583–593.

Lee RH & Heckman CJ (1999). Paradoxical effect of QX-314 on persistent inward currents and bistable behavior in spinal motoneurons in vivo. *J Neurophysiol* **82**, 2518–2527.

Lee RH & Heckman CJ (2000). Adjustable amplification of synaptic input in the dendrites of spinal motoneurons in vivo. *J Neurosci* **20**, 6734–6740.

Lee RH, Kuo JJ, Jiang MC & Heckman CJ (2003). Influence of active dendritic currents on input-output processing in spinal motoneurons in vivo. *J Neurophysiol* **89**, 27–39.

Li Y & Bennett DJ (2003). Persistent sodium and calcium currents cause plateau potentials in motoneurons of chronic spinal rats. *J Neurophysiol* **90**, 857–869.

Li Y, Gorassini MA & Bennett DJ (2004). Role of persistent sodium and calcium currents in motoneuron firing and spasticity in chronic spinal rats. *J Neurophysiol* **91**, 767–783.

Powers RK & Binder MD (1995). Effective synaptic current and motoneuron firing rate modulation. *J Neurophysiol* **74**, 793–801.

Powers RK & Binder MD (2000). Summation of effective synaptic currents and firing rate modulation in cat spinal motoneurons. *J Neurophysiol* **83**, 483–500.

Powers RK & Binder MD (2001). Input-output functions of mammalian motoneurons. *Rev Physiol Biochem Pharmacol* **143**, 137–263.

Prather JF, Powers RK & Cope TC (2001). Amplification and linear summation of synaptic effects on motoneuron firing rate. *J Neurophysiol* **85**, 43–53.

Romaiguere P, Vedel JP, Pagni S & Zenatti A (1989). Physiological properties of the motor units of the wrist extensor muscles in man. *Exp Brain Res* **78**, 51–61.

Rose PK & Cushing S (1999). Non-linear summation of synaptic currents on spinal motoneurons: lessons from simulations of the behaviour of anatomically realistic models. *Prog Brain Res* **123**, 99–107.

Sawczuk A, Powers R & Binder MD (1995). Spike frequency adaptation studied in hypoglossal motoneurons of the rat. *J Neurophysiol* **73**, 1799–1810.

Schwindt PC & Crill WE (1977). A persistent negative resistance in cat lumbar motoneurons. *Brain Res* **120**, 173–178.

Schwindt PC & Crill WE (1982). Factors influencing motoneuron rhythmic firing: results from a voltage-clamp study. *J Neurophysiol* **48**, 875–890.

Segev I, Fleshman JW & Burke RE (1990). Computer simulation of group Ia EPSPs using morphologically realistic models of cat alpha-motoneurons. *J Neurophysiol* **64**, 648–660.

Shapovalov AI (1972). Extrapyramidal monosynaptic and disynaptic control of mammalian alpha-motoneurons. *Brain Res* **40**, 105–115.

Svirskis G & Hounsgaard J (1998). Transmitter regulation of plateau properties in turtle motoneurons. *J Neurophysiol* **79**, 45–50.

Acknowledgements

Funding for this work was provided by the Alberta Heritage Foundation for Medical Research (Alberta, Canada), Canadian Institutes of Health Research (Ontario, Canada), and National Institutes of Health (Maryland, USA) for V. K. Mushahwar.

© 2006 The Authors. Journal compilation © 2006 The Physiological Society